Hybrid double-dot qubit measurement with a quantum point contact*

Yan Lei(严 蕾), Yin Wen(殷 雯)†, and Wang Fang-Wei(王芳卫)

Institute of Physics, Chinese Academy of Sciences, Beijing 100190, *China*

(Received 30 April 2014; revised manuscript received 19 May 2014; published online 10 August 2014)

We present the measurement of a hybrid double-dot qubit using a quantum point contact (QPC). To study the dynamics, we derive the rate equations of the entire system. Numerical results show that QPC current can directly reflect the evolution of the qubit. By adjusting Coulomb interaction, energy mismatch, and QPC tunneling rate, the efficiency and dephasing time can be improved. In addition, the initial state with a hybrid triplet state is superior to that with the purely triplet states on the efficiency. Moreover, the decoherence time is estimated on the magnitude of a microsecond, long enough to implement quantum operations.

Keywords: measurement, dynamics, dephasing

PACS: 03.65.Yz, 03.67.Lx, 73.63.Kv **DOI:** 10.1088/1674-1056/23/10/100303

1. Introduction

Solid state proposals for scalable quantum information processors have attracted considerable interest since they are compatible with existing semiconductor technology.[1,2] The measurement of qubit with high efficiency, as one of the most debated issues in quantum mechanics,[3] is necessary for realizing quantum information processors.[4] An obvious solid candidate of such measurement is a quantum-point contact (QPC).[5] Various theoretical proposals have been put forward on the state measurement with QPC.[6–9] Experimentally, spin state measurements of single and double dots (DDs) have been implemented using QPC through spin-to-charge conversion[10,11] and radio-frequency technique.[12] However, performing a high efficiency measurement in a solid state regime is still very challenging.[9] Therefore, the research on how to improve the effectiveness of the detector by a proper selection of its parameters becomes very important.

Recently, a hybrid double-dot qubit[13] has been promised. It comprises double dots with two electrons confined in one dot and one electron in the other (see Fig. 1). Different from the singlet-triplet qubit[14] and triple-dot qubit,[15] two states of the hybrid qubit with total spin quantum numbers $S = 1/2$ and z component of total spin $S_Z = -1/2$ are $|0\rangle_{\rm L} = |S\rangle|\downarrow\rangle$ and $|1\rangle_{\rm L} = \sqrt{1/3}|T_0\rangle|\downarrow\rangle - \sqrt{2/3}|T_-\rangle|\uparrow\rangle$ named the hybrid triplet state in the following. Here $|S\rangle$, $|T_0\rangle$, and $|T_-\rangle$ are the singlet $((|\uparrow\downarrow\rangle - |\downarrow\uparrow\rangle)/\sqrt{2})$, triplet $((|\uparrow\downarrow\rangle + |\downarrow\uparrow\rangle)/\sqrt{2})$, and triplet $(|\downarrow\downarrow\rangle)$ in left dot respectively. $|\uparrow\rangle$ $(|\downarrow\rangle)$ denotes the spin-up (down) in the right dot. Reference [13] stressed the qubit in Si/SiGe heterostructures combining speed and fabrication simplicity. They mainly presented the large difference in the tunnel rates between the singlet and triplet states in the doubly-occupied (left) dot coupled to the left reservoir and long singlet-triplet relaxation time experimentally.

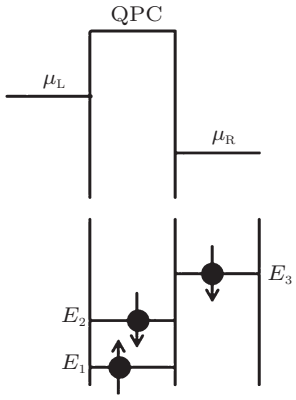


Fig. 1. A diagram of the hybrid double-dot qubit measured by a QPC detector.

In this paper, we focus on the dynamics of the hybrid qubit measured by a QPC theoretically (see Fig. 1). QPC as an electrometer is close to the double-occupied dot. The electrons may oscillate between the dots without spin flipping. S and S_Z are conserved in the process. QPC can measure the oscillation owing to the sensitivity to the electrons nearby. Using the method developed by Gurvitz and Prager,[16,17] we first derive the rate equations for the system. Through the numerical analysis, we find that QPC current can follow the evolution of $|0\rangle_{\rm L}$ state directly. In particular, current-noise power spectrums, which reveal the time correlation between individual electron events,[18] are presented. This allows us to discuss the measurement efficiency for different parameters. Then we conclude how to improve the efficiency and decoherence time briefly, which may be instructive for experiments. Besides, the efficiency of the initial hybrid triplet state is higher than that

*Project supported by the National Natural Science Foundation of China (Grant No. 11174358) and the National Basic Research Program of China (Grant No. 2010CB833102).

†Corresponding author. E-mail: wenyin@aphy.iphy.ac.cn

© 2014 Chinese Physical Society and IOP Publishing Ltd

of the initial purely triplet states. Finally, we evaluate theoretically the dephasing time in the microsecond range, which is long enough for quantum operations.

2. Model and formula

The hybrid DD qubit with a QPC detector is shown in Fig. 1. QPC is represented by a tunneling junction and $\mu_{\rm L}$ ($\mu_{\rm R}$) is the chemical potential in the left (right) reservoir. The hybrid qubit contains three electrons in the DDs for $(2,1)$ charge configuration. Here, (n,m) refers to the number of electrons in the left (n) and right (m) dots. E_1 and E_2 stand for the lowest single particle energies of the left dot and E_3 stands for the lowest single particle energy of the right dot satisfying the condition $E_3 > E_2 > E_1$. The $(2,1)$ configurations always have the lowest energy by adjusting appropriate gate voltage applied to the DDs.[13] Since the state that two electrons with different spins in the level E_2 and one electron in the level E_3 has the highest energy among the $(2,1)$ configuration, we neglect this state for we are only interested in the low energy states. Indeed, we just consider the charge states of the hybrid qubit. According to the models of Refs. [6]–[9], the whole system is described by the following Hamiltonian: $H = H_{\rm DD} + H_{\rm QPC} + H_{\rm int}$. The Hamiltonian for DDs is expressed as

$$\begin{aligned} & H_{\rm DD} \\ = & \sum_{i,\sigma} E_i a^{\dagger}_{i,\sigma} a_{i,\sigma} + U \sum_i n_{i\uparrow} n_{i\downarrow} \\ & + U_1 \sum_{\sigma,\sigma'} n_{1\sigma} n_{2\sigma'} + K \sum_{\sigma,\sigma'} a^{\dagger}_{1,\sigma} a^{\dagger}_{2,\sigma'} a_{1,\sigma'} a_{2,\sigma} \\ & + \frac{\Omega^2}{\Delta_1} \sum_{\sigma,\sigma'} a^{\dagger}_{1,\sigma} a_{3,\sigma} a^{\dagger}_{3,\sigma'} a_{1,\sigma'} + \frac{\Omega^2}{\Delta_2} \sum_{\sigma,\sigma'} a^{\dagger}_{2,\sigma} a_{3,\sigma} a^{\dagger}_{3,\sigma'} a_{2,\sigma'} \\ & + \frac{\Omega^2}{\Delta_3} \left(\sum_{\sigma,\sigma'} a^{\dagger}_{2,\sigma} a_{3,\sigma} a^{\dagger}_{3,\sigma'} a_{1,\sigma'} + \sum_{\sigma,\sigma'} a^{\dagger}_{1,\sigma} a_{3,\sigma} a^{\dagger}_{3,\sigma'} a_{2,\sigma'} \right), \end{aligned} \tag{1}$$

where E_i with $i = 1,2,3$ represents energy levels respectively, $a^{\dagger}_{i,\sigma}(a_{i,\sigma})$ is the creation (annihilation) operator of the electron with spin $\sigma = \uparrow, \downarrow$ in the i energy level, U is the intra-level Coulomb energy, U_1 is the inter-level Coulomb energy, K is intra-dot exchange Coulomb energy, Ω is the inter-dot tunneling amplitude, and $n_{i\sigma} = a^{\dagger}_{i\sigma} a_{i\sigma}$ is the occupation number operator of the i energy level. We have disregarded the inter-dot Coulomb energy because it only provides an energy constant for the system. The last three terms, differing from previous models,[6–9] are second-order tunneling terms and Δ_i with $i = 1,2,3$ is the energy difference between the hopping states.[13] The second-order hopping results in the evolution of the four states through an intermediate state. A very large Coulomb repulsion exists in the triply-occupied quantum dot. So we just take into account the second-order hopping between the charge state $(2,1)$ and $(1,2)$. This induces the transitions between the $|0\rangle_{\rm L}$ and $|1\rangle_{\rm L}$. For simplicity, we assume K and $1/\Delta_i$ are much less than the Coulomb energy U. Then we can safely write the following expression

$$\frac{1}{\Delta_1} = \frac{2}{E_1 - E_3 + U_1 - U}, \quad \frac{1}{\Delta_2} = \frac{2}{E_2 - E_3 + U_1 - U},$$

and

$$\frac{1}{\Delta_3} = \frac{1}{E_2 - E_3 + U_1 - U} + \frac{1}{E_1 - E_3}.$$

This indicates that the larger the energy difference, the less the hopping rate. The Hamiltonian for QPC is given by

$$H_{\rm QPC} = \sum_l E_l c^{\dagger}_l c_l + \sum_r E_r c^{\dagger}_r c_r + \sum_{l,r} \Omega_{lr} \left(c^{\dagger}_l c_r + c^{\dagger}_r c_l \right). \tag{2}$$

Similarly, E_l, E_r and $c^{\dagger}_l(c_l)$, $c^{\dagger}_r(c_r)$ are electron energies and creation (annihilation) operators for the left and right reservoir respectively. The interaction between the DD and QPC is described as

$$\begin{aligned} H_{\rm int} = & \sum_{l,r} \delta\Omega_{lr} a^{\dagger}_{2\uparrow} a_{2\uparrow} \left(c^{\dagger}_l c_r + c^{\dagger}_r c_l \right) \\ & + \sum_{l,r} \delta\Omega_{lr} a^{\dagger}_{2\downarrow} a_{2\downarrow} \left(c^{\dagger}_l c_r + c^{\dagger}_r c_l \right). \end{aligned} \tag{3}$$

The effective QPC tunneling amplitude changes from Ω_{lr} to $\Omega_{lr} + \delta\Omega_{lr}$ when an electron is located in the two levels. In the following, we suppose the tunneling amplitude is independent of spin and energy.

Using the method developed by Gurvitz and Prager,[16,17] we can get the Bloch-type equations of the density matrix $\sigma^n_{ij}(t)$. In this notation, i, j denote all available discrete states of the DDs and n represents the number of electrons arriving at the right reservoir by the time t. As shown in Fig. 2, there are four possible states labeled by $1,2,3,4$. $|1\rangle$ denotes the electron with spin up in the level E_1 and the others in the levels E_2 and E_3; $|2\rangle$ denotes the electron with spin up in the level E_2 and the others in the levels E_1 and E_3; $|3\rangle$ denotes the electron with spin up in the level E_3 and the others in the levels E_1 and E_2; $|4\rangle$ denotes the two electrons with different spins in the level E_1 and the other in the level E_3. Obviously, the superposition of $|1\rangle$, $|2\rangle$, and $|3\rangle$ is the logical state $|1\rangle_{\rm L}$ and $|4\rangle$ refers to the logical state $|0\rangle_{\rm L}$.

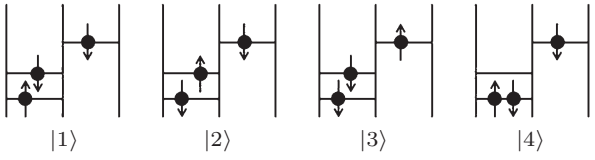


Fig. 2. All available electron states of the DDs.

The dynamics of the whole system is governed by the following equations:

$$\dot{\sigma}^n_{11} = -\Gamma_1 \sigma^n_{11} + \Gamma_1 \sigma^{n-1}_{11} + {\rm i}K(\sigma^n_{21} - \sigma^n_{12})$$

$$+\mathrm{i}\frac{\Omega^2}{\Delta_1}(\sigma_{31}^n-\sigma_{13}^n), \tag{4a}$$

$$\dot{\sigma}_{22}^n = -\Gamma_1\sigma_{22}^n+\Gamma_1\sigma_{22}^{n-1}+\mathrm{i}K(\sigma_{12}^n-\sigma_{21}^n) +\mathrm{i}\frac{\Omega^2}{\Delta_2}(\sigma_{32}^n-\sigma_{23}^n)+\mathrm{i}\frac{\Omega^2}{\Delta_3}(\sigma_{42}^n-\sigma_{24}^n), \tag{4b}$$

$$\dot{\sigma}_{33}^n = -\Gamma_1\sigma_{33}^n+\Gamma_1\sigma_{33}^{n-1}+\mathrm{i}\frac{\Omega^2}{\Delta_1}(\sigma_{13}^n-\sigma_{31}^n) +\mathrm{i}\frac{\Omega^2}{\Delta_2}(\sigma_{23}^n-\sigma_{32}^n)-\mathrm{i}\frac{\Omega^2}{\Delta_3}(\sigma_{43}^n-\sigma_{34}^n), \tag{4c}$$

$$\dot{\sigma}_{44}^n = -\Gamma\sigma_{44}^n+\Gamma\sigma_{44}^{n-1}+\mathrm{i}\frac{\Omega^2}{\Delta_3}(\sigma_{24}^n-\sigma_{42}^n) -\mathrm{i}\frac{\Omega^2}{\Delta_3}(\sigma_{34}^n-\sigma_{43}^n), \tag{4d}$$

$$\dot{\sigma}_{12}^n = \mathrm{i}\left(\frac{\Omega^2}{\Delta_2}-\frac{\Omega^2}{\Delta_1}\right)\sigma_{12}^n-\Gamma_1\sigma_{12}^n+\Gamma_1\sigma_{12}^{n-1}+\mathrm{i}K(\sigma_{22}^n-\sigma_{11}^n) +\mathrm{i}\frac{\Omega^2}{\Delta_1}\sigma_{32}^n-\mathrm{i}\frac{\Omega^2}{\Delta_2}\sigma_{13}^n-\mathrm{i}\frac{\Omega^2}{\Delta_3}\sigma_{14}^n, \tag{4e}$$

$$\dot{\sigma}_{13}^n = \mathrm{i}\left(\frac{\Omega^2}{\Delta_2}-K\right)\sigma_{13}^n-\Gamma_1\sigma_{13}^n+\Gamma_1\sigma_{13}^{n-1}+\mathrm{i}K\sigma_{23}^n +\mathrm{i}\frac{\Omega^2}{\Delta_1}(\sigma_{33}^n-\sigma_{11}^n)-\mathrm{i}\frac{\Omega^2}{\Delta_2}\sigma_{12}^n+\mathrm{i}\frac{\Omega^2}{\Delta_3}\sigma_{14}^n, \tag{4f}$$

$$\dot{\sigma}_{14}^n = \mathrm{i}\left(E_1-E_2+U-U_1-\frac{\Gamma+\Gamma_1}{2}\right)\sigma_{14}^n+\sqrt{\Gamma_1\Gamma}\sigma_{14}^{n-1} +\mathrm{i}K\sigma_{24}^n+\mathrm{i}\frac{\Omega^2}{\Delta_1}\sigma_{34}^n-\mathrm{i}\frac{\Omega^2}{\Delta_3}\sigma_{12}^n+\mathrm{i}\frac{\Omega^2}{\Delta_3}\sigma_{13}^n, \tag{4g}$$

$$\dot{\sigma}_{23}^n = \mathrm{i}\left(\frac{\Omega^2}{\Delta_1}-K\right)\sigma_{23}^n-\Gamma_1\sigma_{23}^n+\Gamma_1\sigma_{23}^{n-1}+\mathrm{i}K\sigma_{13}^n +\mathrm{i}\frac{\Omega^2}{\Delta_2}(\sigma_{33}^n-\sigma_{22}^n)+\mathrm{i}\frac{\Omega^2}{\Delta_3}(\sigma_{43}^n+\sigma_{24}^n)-\mathrm{i}\frac{\Omega^2}{\Delta_1}\sigma_{21}^n, \tag{4h}$$

$$\dot{\sigma}_{24}^n = \mathrm{i}\left(E_1-E_2+U-U_1+\frac{\Omega^2}{\Delta_1}-\frac{\Omega^2}{\Delta_2}-\frac{\Gamma+\Gamma_1}{2}\right)\sigma_{24}^n +\sqrt{\Gamma_1\Gamma}\sigma_{24}^{n-1}+\mathrm{i}K\sigma_{14}^n+\mathrm{i}\frac{\Omega^2}{\Delta_2}\sigma_{34}^n +\mathrm{i}\frac{\Omega^2}{\Delta_3}(\sigma_{44}^n-\sigma_{22}^n+\sigma_{23}^n), \tag{4i}$$

$$\dot{\sigma}_{34}^n = \mathrm{i}\left(E_1-E_2+U-U_1+K-\frac{\Omega^2}{\Delta_2}-\frac{\Gamma+\Gamma_1}{2}\right)\sigma_{34}^n +\sqrt{\Gamma_1\Gamma}\sigma_{34}^{n-1}+\mathrm{i}\frac{\Omega^2}{\Delta_1}\sigma_{14}^n+\mathrm{i}\frac{\Omega^2}{\Delta_2}\sigma_{24}^n +\mathrm{i}\frac{\Omega^2}{\Delta_3}(\sigma_{33}^n-\sigma_{44}^n-\sigma_{32}^n), \tag{4j}$$

where

$$\Gamma = 2\pi\rho_{\mathrm{L}}\rho_{\mathrm{R}}\Omega_{lr}^2(\mu_{\mathrm{L}}-\mu_{\mathrm{R}})$$

and

$$\Gamma_1 = 2\pi\rho_{\mathrm{L}}\rho_{\mathrm{R}}(\Omega_{lr}+\delta\Omega_{lr})^2(\mu_{\mathrm{L}}-\mu_{\mathrm{R}})$$

correspond to the QPC tunneling rates when zero and one electron occupy the level E_2 respectively. Since the states in the reservoirs are very dense (continuum), $\rho_{\mathrm{L(R)}}$ is the density of states in the left (right) reservoir.

The qubit behavior is obtained from the reduced density matrix by tracing out the detector variable n: $\sigma_{ij}(t)=\sum_n\sigma_{ij}^n(t)$. On the other hand, the detector behavior is depicted by tracing out the qubit variable: $P_n(t)=\sum_j\sigma_{jj}^n(t)$. This quantity is the probability of n electrons arriving at the right reservoir. We can further get the average QPC current[8]

$$I(t)=e\sum_n n\dot{P}_n(t)=e\Gamma_1(\sigma_{11}+\sigma_{22}+\sigma_{33})+e\Gamma\sigma_{44}, \tag{5}$$

and the noise power spectrum of the current fluctuations based on the MacDonald's formula[19,20]

$$S(\omega)=2e^2\omega\int_0^\infty \mathrm{d}t\sum_n n^2\dot{P}_n(t)\sin(\omega t). \tag{6}$$

Noise power spectrum is a unique tool to probe more information which is not available for the average current.[18] From Eqs. (4) and (6) we can acquire that

$$S(\omega)=2e^2\omega\mathrm{Im}[\Gamma_1(Z_{11}+Z_{22}+Z_{33})+\Gamma Z_{44}], \tag{7}$$

where $Z_{jj}(\omega)=\int_0^\infty \mathrm{d}t\sum_n(2n+1)\sigma_{jj}^n(t)\exp(\mathrm{i}wt)$. By reducing Eq. (4) to a set of linear algebraic equations after the integration over t, we can calculate these quantities.

3. Dynamics and measurement efficiency

It is important to understand the dynamics for improving qubit performance.[15] To study the dynamics of the qubit, we make numerical analysis by solving the rate equations regarding the reduced density matrix $\sigma_{ij}(t)$. In this section, we set electrons in the $|3\rangle$ state initially. This is supported by the large difference in tunnel rates between the singlet and triplet states of the left dot coupled to the left reservoir, which has been proved in Si[13] and GaAs.[21] To facilitate the description, E_1 and Ω are chosen as the energy zero point and the energy unit correspondingly. We assume that the Coulomb interactions satisfy the relation $U=2U_1$. First, we set $U=40$, $E_2=4$, and $E_3=8$ to ensure $(2,1)$ charge states with the lowest energy. To make $K\ll U$ as mentioned above, we chose $K=0.1$. The time evolution of σ_{11} and σ_{22} is roughly the same as shown in Fig. 3(a) and Fig. 3(b), because the hopping rates of electrons between the levels E_1, E_2, and E_3 are approximately the same. The oscillation frequency of σ_{33} equals that of σ_{11} and σ_{22}, while the phase is opposite (see Fig. 3(c)). Destructive interference occurs between the states $|1\rangle$, $|2\rangle$, and $|3\rangle$ due to the measurement-caused dephasing. If we compare Fig. 3(d) with Fig. 3(e), we find that time-dependent QPC current is in line with the evolution of σ_{44}. Two insets show that even the small oscillation for σ_{44} can be detected by the QPC. In other words, the $|0\rangle_{\mathrm{L}}$ state of hybrid qubit can be read out directly from the QPC current.

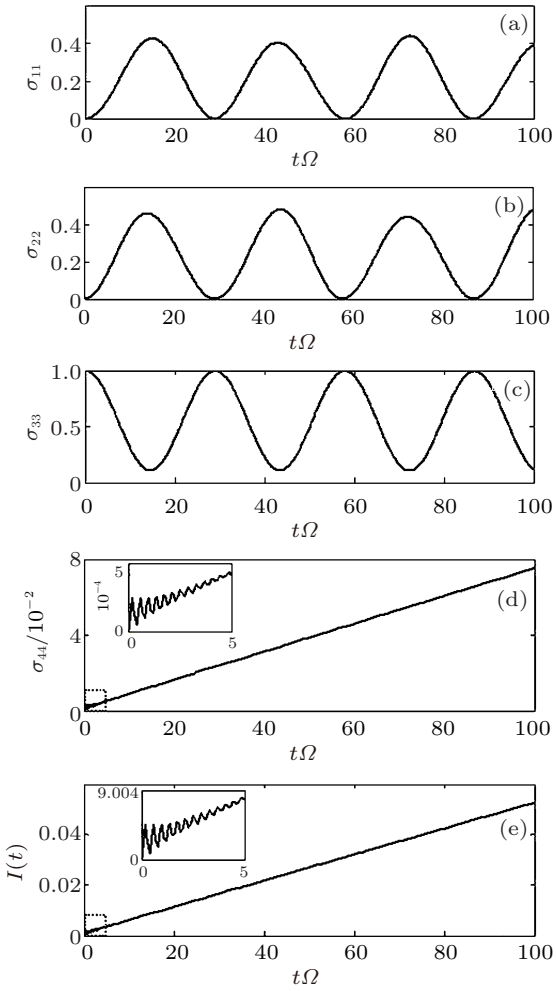


Fig. 3. The time evolution of electron occupation probability σ_{11} (a), σ_{22} (b), σ_{33} (c), σ_{44} (d), and QPC current $I(t)$ (e) with the tunneling rate $\Gamma = 16$ and $\Gamma_1 = 9$. Insets: zoom in on the dashed area of the counterpart region in panels (d) and (e).

In the presence of dephasing, current noise attracts our attention due to the possibility of extracting information of the system parameters that govern the dynamics of the system.[22] Current-noise power spectrum reveals both coherent dynamics from the qubit and incoherent dynamics stemming from the detector.[23] Also, the peak-to-background ratio of the current noise spectrum is a measure of the measurement efficiency.[24] Motivated by these, we analyze the current-noise power spectrum numerically. Here we take the normalized current-noise power spectrum $S(\omega)/S_0$,[23] where $S(\omega)$ is expressed analytically in Eq. (7) and $S_0 = 2e\bar{I}$. $\bar{I}$ is the steady current of QPC. In what follows, we mainly discuss how to improve the measurement efficiency.

Coulomb interaction plays an important role in our model so we first discuss its effects on the system. The larger the Coulomb interaction U, the lower the hopping rate. When U is increased, the oscillation of electrons slows down and consequently dephasing time prolongs as shown in Fig. 4(a). Since the QPC current measures the electron occupation probability σ_{44} which has higher frequency than others, hereafter we only consider the frequency part of the noise spectrum related to σ_{44}. In Fig. 4(b), for larger Coulomb interaction, the peak corresponding to the Rabi frequency is less pronounced and the oscillation frequency is higher. We speculate that the Coulomb interaction tends to locate the electrons leading to suppressed charge fluctuation. The increasing frequency may result from the higher energy of $|4\rangle$ accelerating oscillation. To conclude, on condition that the Coulomb repulsion U is much larger than the exchange Coulomb energy K and hopping amplitude, decreasing U can raise the measurement efficiency, but shorten the decoherence time. That is, we should accommodate Coulomb energy U to trade off both effectiveness and coherence.

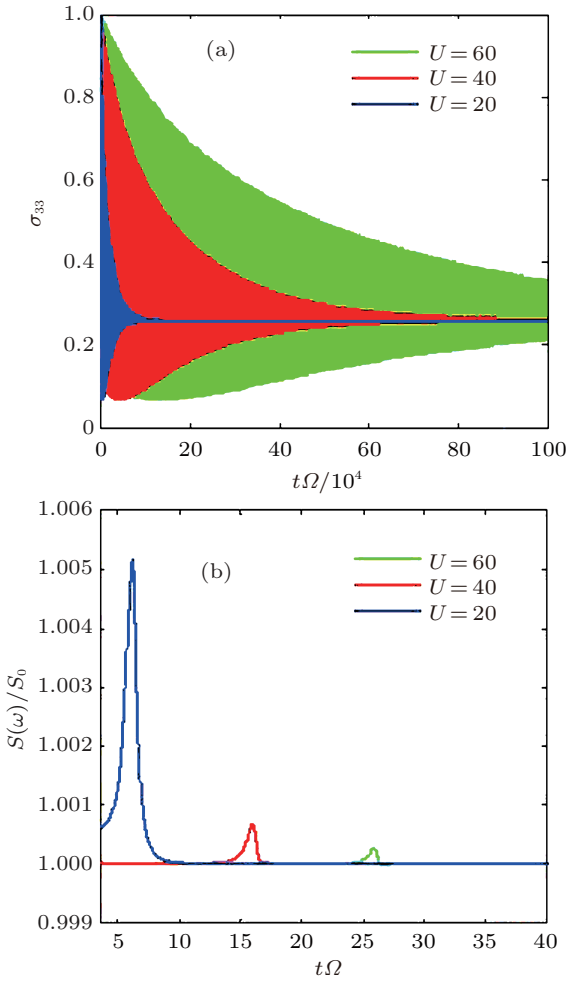


Fig. 4. (color online) The electron occupation probability σ_{33} (a) as a function of time and normalized current-noise power spectrum $S(\omega)/S_0$ (b) as a function of frequency with different Coulomb interactions: $U = 60$ (green), $U = 40$ (red), and $U = 20$ (blue).

Next, we discuss the impact of energy mismatch on the system performance. Parameters are set as $U = 40$, $\Gamma = 16$, and $\Gamma_1 = 9$. Fixing $E_3 = 20$, level E_2 varies between E_1 and E_3. When E_2 is closer to E_3, both decoherence rate and peak-to-background ratio are increased[25] as shown in Fig. 5(a) and Fig. 5(b). Similarly, if level E_3 is changed above the $E_2 = 4$,

a similar effect occurs when E_3 is close to E_2 (see Fig. 5(c) and Fig. 5(d)). However, the latter effect is more obvious. Decreasing E_3 makes the hopping rate of electrons in the levels E_1 and E_2 increase. The charge fluctuation further increases. While increasing E_2 just makes that of E_2 increase, the effect is not conspicuous. In brief, decreasing the energy gap between levels E_3 and E_1, E_2 could improve the measurement efficiency at a cost of shortening the dephasing time. This can be implemented by tuning the gate voltages of the two dots.[26]

Apart from the factors of DDs qubit as mentioned above, QPC as a noise source would dissipate the qubit. We keep $U = 40$, $E_2 = 4$, $E_3 = 10$, and $\Gamma_1 = 9$. From Eqs. (4), with an increase of the tunneling rate Γ, the decoherence rate increases. In addition, σ_{44} potentially has a classical incoherence behavior for large Γ as shown in Fig. 6(a). In principle, we can distinguish classical and quantum behavior by monitoring the peaks in the noise spectrum.[23] Figure 6(b) shows the noise spectrums for different QPC tunneling rates Γ. The peak in the spectrum broadens for the large tunneling rate. This means that quantum coherent oscillation of σ_{44} is suppressed (see Fig. 6(a)). If Γ is large enough, the peak would eventually disappear and σ_{44} would raise in a linear way.[27] So we should try to decrease the QPC tunneling rate thereby lowering the decoherence caused by the measurement. Whereas the tunneling rate is proportional to voltage bias $V = \mu_L - \mu_R$, lowering the bias of QPC can diminish it. Nonetheless, the approach we have used in Section 2 requires the big bias limit $eV \gg \Omega^2 \rho_{L(R)}$.[28] So the bias should be controlled in this limit. On the other hand, Γ should be obviously more than Γ_1, otherwise the measurement would be unambiguous.[29]

By now, we just consider the electrons initialized in the triplet state $|T_-\rangle$. Figure 7 displays the noise power spectrums for initial state $|1\rangle_L$, $|T_-\rangle$, and $|T_0\rangle$. Hybrid state $|1\rangle_L$ reveals the higher measurement efficiency. Indeed, the steady states vary for different initial states. Moreover, if we chose the $\Omega = 10$ GHz,[30] dephasing time due to charge noise is about 1 μs based on Fig. 4(a), Fig. 5(a), and Fig. 5(c), which has the same magnitude with electron–phonon dephasing term.[31] So the charge noise should not be neglected simply. Compared with a typical gate time 1 ns,[32] the decoherence time is considerably long for quantum operations.

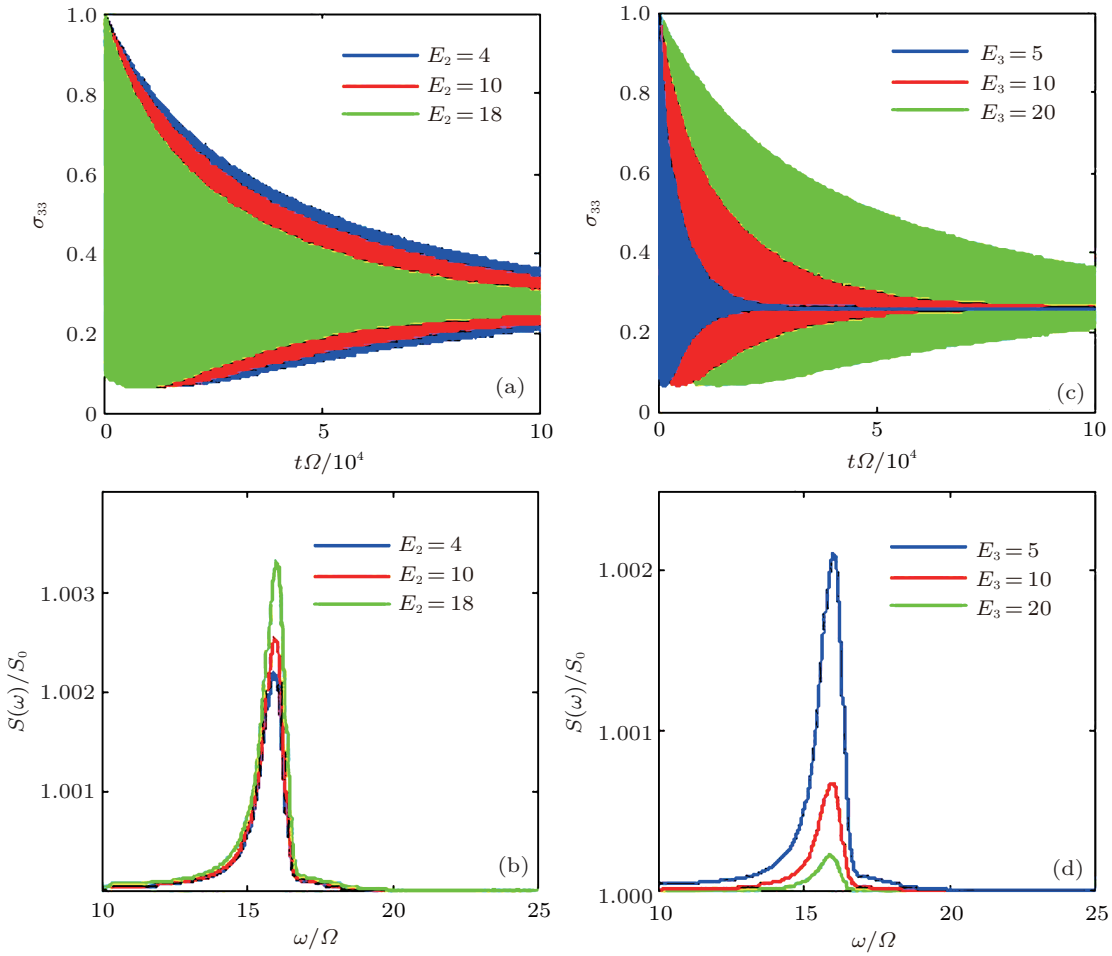


Fig. 5. (color online) The time evolution of σ_{33} (a) and the shot-noise power spectrum $S(\omega)/S_0$ (b) versus frequency for different E_2: $E_2 = 4$ (blue), $E_2 = 10$ (red), and $E_2 = 18$ (green) with $E_3 = 20$. The time-dependent σ_{33} (c) and the shot-noise power spectrum $S(\omega)/S_0$ (d) for different E_3: $E_3 = 5$ (blue), $E_3 = 10$ (red), and $E_3 = 20$ (green) with $E_2 = 4$.

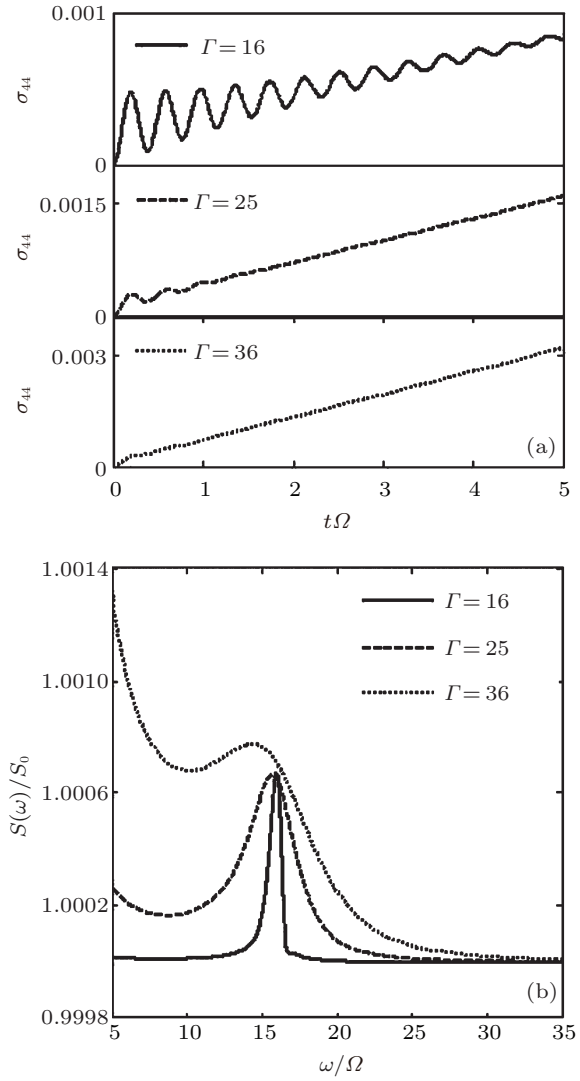


Fig. 6. The time evolution of σ_{44} (a) and shot-noise power spectrum $S(\omega)/S_0$ (b) for different QPC tunneling rates $\Gamma = 16$ (solid), $\Gamma = 25$ (dashed), and $\Gamma = 36$ (dotted).

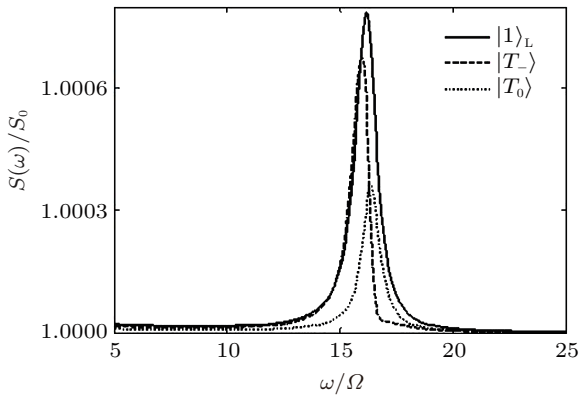


Fig. 7. Shot-noise power spectrum for different initial states: $|1\rangle_{\rm L}$ (solid), triplet $|T_-\rangle$ (dashed), and $|T_0\rangle$ (dotted).

4. Summary and discussion

In conclusion, we proposed a model of measuring a hybrid DD qubit using a QPC. We first derived the Bloch-type rate equations and discussed the dynamics of the system. The numerical analysis shows that QPC current can read out directly the evolution of the qubit. Then we discussed how to improve the measurement effectiveness and dephasing time. Decreasing the Coulumb interaction and the mismatch between energy level E_3 and others can increase the efficiency, but these make the decoherence time decline. We reiterate that the results based on that Coulomb repulsion U are much larger than exchange Coulomb energy K and hopping amplitude. To obtain the useful quantum information, we should reduce the QPC tunneling rate on the big bias limit $eV \gg \Omega^2\rho_{\rm L,R}$. In addition, the qubit initialized in the hybrid triplet state displays a higher efficiency than that in purely triplet states, which is another advantage of the hybrid qubit. Moreover, the dephasing time is estimated on the magnitude of a microsecond, which is long enough for quantum operations. We expect that these results will ease the hard path to realize the quantum computation in the laboratory.

To identify our results, we hope experimenters can study the quantum evolution about our model. One method is the so-called free induction decay. Specifically, the voltage pulses applied to the gate initialize, evolve, and read out the qubit.[14] A radio-frequency technique can also be used for our model. That is, QPC is embedded in a resonant circuit.[33,34]

Yet, from the above discussion, we note that the peak-to-background ratio of the noise power spectrum is always roughly 1, which is less than an ideal detector yielding a ratio of 4.[6,24] In practice, the frequency noise power spectrum is difficult to measure. However it is appealing because it includes information about the full dynamics of the system.[23] So we should make further efforts to improve measurement efficiency. In theory, various suggestions about the quantum operation and algorithm for this new-type qubit need to be investigated in the future.

References

[1] Kane B E 1998 *Nature* **393** 133
[2] Loss D and DiVincenzo D P 1998 *Phys. Rev. A* **57** 120
[3] ClarkeEur M L 2014 *J. Phys.* **35** 015021
[4] DiVincenzo D P 2000 *Fortschr. Phys.* **48** 771
[5] Mozyrsky D and Martin I 2002 *Phys. Rev. Lett.* **89** 018301
[6] Goan H S, Milburn G J, Wiseman H M and Sun H B 2001 *Phys. Rev. B* **63** 125326
[7] Gurvitz S A 2005 *Phys. Rev. B* **72** 073303
[8] Gilad T and Gurvitz S A 2006 *Phys. Rev. Lett.* **97** 116806
[9] Goan H S and Milburn G J 2001 *Phys. Rev. B* **64** 235307
[10] Elzerman J M, Hanson R, van Willems, Beveren L H, Witkamp B, Vandersypen L M K and Kouwenhoven L P 2004 *Nature* **430** 431
[11] Johnson A C, Petta J R, Taylor J M, Yacoby A, Lukin M D, Marcus C M, Hanson M P and Gossard A C 2005 *Nature* **435** 925
[12] Petersson K D, Smith C G, Anderson D, Atkinson P, Jones G A C and Ritchie D A 2010 *Nano Lett.* **10** 2789
[13] Shi Z, Simmons C B, Prance J R, Gamble J K, Koh T S, Shim Y P, Hu X, Savage D E, Lagally M G, Eriksson M A, Friesen M and Coppersmith S N 2012 *Phys. Rev. Lett.* **108** 140503
[14] Dial O E, Shulman M D, Harvey S P, Bluhm H, Umansky V and Yacoby A 2013 *Phys. Rev. Lett.* **110** 146804

[15] DiVincenzo D P, Bacon D, Kempe J, Burkard G and Whaley K B 2000 *Nature* **408** 339
[16] Gurvitz S A and Prager Ya S 1996 *Phys. Rev. B* **53** 15932
[17] Gurvitz S A 1997 *Phys. Rev. B* **56** 15215
[18] Blanter Ya M and Büttiker M 2000 *Phys. Rep.* **336** 1
[19] MacDonald D K C 1948 *Rep. Prog. Phys.* **12** 56
[20] Mozyrsky D, Fedichkin L, Gurvitz S A and Berman G P 2002 *Phys. Rev. B* **66** 161313
[21] Hanson R, van Beveren L H W, Vink I T, Elzerman J M, Naber W J M, Koppens F H L, Kouwenhoven L P and Vandersypen L M K 2005 *Phys. Rev. Lett.* **94** 196802
[22] Luo J Y, Li X Q and Yan Y J 2007 *Phys. Rev. B* **76** 085325
[23] Korotkov A N 2001 *Phys. Rev. B* **63** 085312
[24] Lambert N and Nori F 2008 *Phys. Rev. B* **78** 214302
[25] Elattari B and Gurvitz S A 2002 *Phys. Lett. A* **292** 289
[26] Bennett C H 1995 *Phys. Today* **48** 24
[27] Korotkov A N and Averin D V 2001 *Phys. Rev. B* **64** 165310
[28] Elattari B and Gurvitz S A 2000 *Phys. Rev. A* **62** 032102
[29] Lundeen J S and Bamber C 2012 *Phys. Rev. Lett.* **108** 070402
[30] Gustavsson S, Studer M, Leturcq R, Ihn T, Ensslin K, Driscoll D C and Gossard A C 2007 *Phys. Rev. Lett.* **99** 206804
[31] Gamble J K, Friesen M, Coppersmith S N and Hu X 2012 *Phys. Rev. B* **86** 035302
[32] Petersson K D, Petta J R, Lu H and Gossard A C 2010 *Phys. Rev. Lett.* **105** 246804
[33] Yan L, Wang H X, Yin W and Wang F W 2014 *Chin. Phys. B* **23** 020305
[34] Cassidy M C, Dzurak A S, Clark R G, Petersson K D, Farrer I, Ritchie D A and Smith C G 2007 *Appl. Phys. Lett.* **91** 222104